

IMECE2007-41076

**DRAFT: MODELING INSECT FILIFORM HAIR MOTION USING THE PENALTY
IMMERSED BOUNDARY METHOD**

Tomáš Gedeon*

Department of Mathematics
and
Center for Computational Biology
Montana State University
Bozeman, Montana 59715
Email: gedeon@math.montana.edu

Jeff J. Heys and B.C. Knott

Chemical Engineering Department
Arizona State University
Tempe, AZ 85287-6006
Email: jheys@asu.edu

Jonas Mulder-Rosi

Center for Computational Biology
Montana State University
Bozeman, Montana 59715
Email: jmulderr@gmail.com

ABSTRACT

*Many insects are able to sense their surrounding fluid environment through induced motion of their filiform hairs. The mechanism by which the insect can sense a wide range of input signals using the canopy of filiform hairs of different length and orientation is of great interest. Most of the previous filiform hair models have focused on a single, rigid hair in an idealized air field. We have developed [1] a model for a canopy of filiform hairs that are mechanically coupled to the surrounding air. The model equations are based on the penalty immersed boundary method. The key difference between the penalty immersed boundary method and the traditional immersed boundary method is the addition of forces to account for density differences between the immersed solid (the filiform hairs) and the surrounding fluid (air). In this work we validate the model by comparing the model predictions to experimental results on cricket *Acheta domestica* cercal system.*

NOMENCLATURE

cerci Cone-like appendages at the rear end of a cricket.
filiform hair Thread-like hair.

Introduction

Many biological systems test the limits of our understanding of fluid-structure interactions. Insect air-current receptors serve as an example of this challenge. These receptors consist of multiple thread-like filiform hairs (see figure 1) that move in response to air current. Each hair is attached to a sensory neuron, that transmits the information about the air currents to the brain. The principal difficulties in modelling the fluid-structure interaction in this case are the large number of the hairs and their essentially 1-dimensional character. While the effect of the moving fluid on a single hair can be modelled in a relatively straightforward manner, the effect of the moving hairs on the motion of the fluid is a more formidable challenge. The resulting viscous coupling between the hairs is biologically very important, since it may have a substantial effect on the function of the sensory system and hence very likely poses an evolutionary constraint on development of this system.

In this contribution we review a penalty immersed boundary method, introduced in [1], which allow us to model a fully interacting set of hairs in a fluid. The key difference between the penalty immersed boundary method and the traditional immersed boundary method is the addition of forces to account for density differences between the immersed solid (the filiform hairs) and the surrounding fluid (air). Our model has a single free parameter which we fit to reproduce the data from a cercal system of a cricket *Acheta domestica*.

A number of mathematical models have been developed to

*Address all correspondence to this author.

help describe the relationship between filiform hair structure and its response to various stimuli. In order to compare and contrast our work with that of previous researchers, we briefly review some of these models.

Single hair models

One of the earliest models was proposed in a series of papers by Shimozawa and Kanou [2, 3]. The model was developed by assuming that the filiform could be approximated as an inverted, rigid pendulum with both a viscous- and a spring-type elements to resist angular displacement. The equation of motion describing the motion of the filiform hair under this assumption is

$$I \cdot \frac{d^2\theta}{dt^2} + R \cdot \frac{d\theta}{dt} + S \cdot \theta = N, \quad (1)$$

where I is the moment of inertia of the hair, R is the viscous resistance within the hair base, S is the spring stiffness, and N is the torque applied by the moving air. The R and S parameters were determined through experiments on filiform hairs [3–5], and N was approximated using Stokes’s solution to flow above a large oscillating plate. In this approach the cercus surface was approximated as an infinite plane.

In a series of papers [6–8] Humphrey *et al.* modified Shimozawa’s model. The principal differences between the models are the addition of a ‘virtual mass’ term that captures the effects of fluid inertia and the use of an alternative theory (also by Stokes) for estimating the drag force on the pendulum. In this approach the underlying surface is modelled as an infinite cylinder. However, neither Shimozawa nor Humphrey in this early work model viscosity mediated interactions between the hairs.

The set of models describing single hair motion under the fluid motion is now well established. These models have been used more recently by Shimozawa *et al.* [4, 5] to examine the effects of varying the filiform hair shape on its motion.

Interactions between the hairs

As mentioned in the introduction, modelling viscosity mediated coupling between the hairs presents certain challenges. The models addressing the interaction between the hairs has been developed only very recently. Bathellier *et al.* [9] developed methods for modifying the idealized flow field around a hair to approximate the viscous dampening of the hair on the fluid in order to approximate hair-to-hair coupling. This model is limited to interactions between two hairs.

Most recently, Cummins *et al.* [10] developed the first comprehensive model that allows study of fluid mediated viscous interaction between arbitrary number of hairs. Their model builds on Humphrey’s model in treating the cercus as an infinite cylinder and allowing only periodic fluid motion in the axial direction.

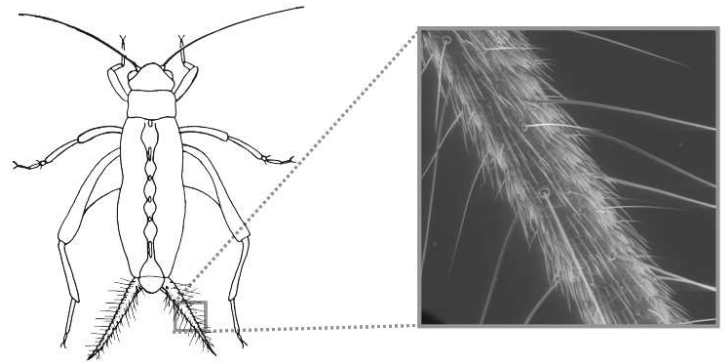


Figure 1. FILIFORM HAIRS ON THE CRICKET CERCI. THE CRICKET HAS A PAIR OF ABDOMINAL CERCI THAT CONTAIN 500-1000 HAIRS EACH. *Foto courtesy of J.P. Miller, Center for Computational Biology, Montana State University*

The fluid velocity is then a sum of an explicit solution of oscillating Navier-Stokes equations over an infinite cylinder and a perturbation velocity due to the presence of hairs. The perturbation velocity is computed using steady Stokes flow approximation to Navier-Stokes equations. Because of the steady state approximation, the model is accurate only for low and moderate frequencies of the driving fluid and a for relatively short distances between the hairs.

Summary of the existing models In summary, the following assumptions are used in models of filiform hair motion:

1. the hairs are rigid, linear oscillators,
2. angular motion of the hair is restricted by a viscous- and spring-type resistance elements at the base,
3. the cercus is a smooth cylinder or infinite plane,
4. often, there is no hair-to-hair interaction, and
5. the bulk flow is oscillatory.

The model of the cercus and filiform hairs presented in the next section was developed to avoid making some of the assumption in the Humphrey and Cummins models. Specifically, arbitrary driving flow from arbitrary direction is allowed, the hairs do not have to be completely rigid, and the bulk flow is determined by solving the Navier-Stokes equations rather than its approximation, or assuming a specific analytical form. The hair-to-hair viscous coupling is captured.

While the hair response to a bulk oscillatory flow is an important problem, there are examples of small scale flow structures, such as microturbulence, being used for communication. Eventually, a model that can capture these structures in the fluid may improve our understanding of cricket-to-cricket communication. Our model is a step in this direction.

We fit our model to data from common cricket (*Acheta domestica*), which we describe next.

Cercal sensory system in a cricket

A cerci of an adult crickets contains 500-1000 filiform hairs each [11]. The length of the wind-receptor hairs vary between 30 and 1500 μm [12], and the hair density is higher near the abdomen relative to the posterior end of the cercus. The hair diameter varies not only between different hairs (from 1 to 9 μm), but also from the tip to the base (with the square root of distance from the tip, [12]). Even though the size and shape of the filiform hairs is highly variable, the inter-animal variability is apparently extremely low [11, 13, 14]. Filiform hairs are placed in oval shaped asymmetrical sockets. The hair pivots in the sockets; the structure of the base of the hair within the socket acts as a hinge, and constrains the motion of the hair to a single plane. This plane varies from hair to hair [11, 13, 14]. At the base of each filiform hair is a single mechanoreceptor neuron that senses the deflection of the hair. The cricket receives information about the velocity, frequency, and direction of air movement through the array of filiform hairs.

Penalty Immersed Boundary Method

In this section we describe the penalty immersed boundary method. The equations of motion for a three-dimensional viscous incompressible fluid are [15]

$$\rho \left(\frac{\partial \mathbf{u}}{\partial t} + \mathbf{u} \cdot \nabla \mathbf{u} \right) = -\nabla p + \mu \Delta \mathbf{u} + \mathbf{f}, \quad (2)$$

$$\nabla \cdot \mathbf{u} = 0, \quad (3)$$

where \mathbf{u} and p are the velocity and pressure of the fluid. At 20°C the viscosity (μ) and density (ρ) of air are $1.8 \times 10^{-5} \text{ kg}/(\text{m}\cdot\text{s})$ and $1.2 \text{ kg}/\text{m}^3$ respectively. Selecting a characteristic velocity, V_0 , of 0.01 m/s and a characteristic length scale, L , of $1 \times 10^{-3} \text{ m}$ gives a Reynolds number of

$$Re = \frac{LV_0\rho}{\mu} = 0.67. \quad (4)$$

A more appropriate characteristic length scale may be the diameter of the hair ($L = 5 \times 10^{-6} \text{ m}$), which gives $Re = 3.3 \times 10^{-3}$. In either case, the term on the left side of equation 2 is likely to be small, but it will be retained because it does not contribute significantly to the computational costs of the algorithm employed

here. The body force term, \mathbf{f} , on the left side is going to be significant in what follows because this term will capture the effects of the immersed, elastic boundary with mass.

The immersed boundary method [15–18] treats the entire domain as a fluid. One- and two-dimensional boundaries without any volume are then 'immersed' in that fluid and coupled to the fluid through a force balance and a velocity matching condition. Originally, the immersed boundary method was developed to model the interaction between a tissue and a biological fluid. Because tissues typically have a density equal to that of biological fluids (i.e., approximately the density of water), the mass of the tissue is treated implicitly because it is the same as the fluid now occupying that volume. Hence, the only force that the immersed boundary applies to the fluid arise from the elastic stress of the material. The filiform hairs of present interest, however, have a much higher density than the surrounding air, and an additional body force must be applied to the fluid to account for the inertia of the hairs and the force of gravity. One mechanism for handling the boundary mass is to locally increase the density of the fluid (i.e., air) so that it is equal to the mass of the immersed boundary, but this approach makes Fourier methods inapplicable [19]. Another approach, which is used here, is to introduce duplicate immersed boundary points (i.e., a second immersed boundary) with mass wherever it is needed. This *massive* boundary accounts for inertia and the gravitational force, and it is connected to the elastic boundary using a strong restoring force. In summary, there are two immersed boundaries, which are tightly linked together, with one boundary without mass representing the elastic forces in the solid and the other massive boundary representing the inertial and gravitation forces. A detailed derivation and analysis of this technique has been published elsewhere [20], and only the details relevant to modelling filiform hairs are presented below.

The velocity of the fluid, $\mathbf{u}(\mathbf{x})$, is expressed in an Eulerian reference frame, and it is defined on the fixed fluid grid. The immersed boundary is based on a Lagrangian reference frame, and its position in time t is given by $\mathbf{X}(r,s,t)$ for the 2-dimensional boundary representing the cercus and by $\mathbf{X}(s,t)$ for the 1-dimensional boundary representing the hairs. We will use the more general notation $\mathbf{X}(r,s,t)$ to explain concepts applicable to both types of boundary. The body force per unit volume on the fluid, \mathbf{f} , is related to the force density in the immersed boundary, \mathbf{F} , by

$$\mathbf{f}(\mathbf{x},t) = \int \mathbf{F}(r,s,t) \delta(\mathbf{x} - \mathbf{X}(r,s,t)) dr ds, \quad (5)$$

where δ is the 3-dimensional Dirac delta function. In calculations we use discrete or distributed delta function, with non-zero symmetric support centred at $\mathbf{X}(r,s,t)$ that is large enough so that it overlaps with the nearest fluid points. Equation 5 is the key equation that handles the interaction between the moving immersed boundary (hairs) and the fluid.

The immersed boundary force density can be divided into two parts: \mathbf{F}_E representing the elastic stress force and \mathbf{F}_K representing the inertial gravitational force. The elastic contribution is given by:

$$\mathbf{F}_E = -\frac{\partial E}{\partial \mathbf{X}}, \quad (6)$$

where $E(\mathbf{X})$ is the elastic energy function. Since each component of a 1-D immersed boundary represents a hair, that can be modelled as a 1-D rod, we use the following energy functional:

$$E(\mathbf{X}(s,t)) = \frac{1}{2}c_s \int \left(\left| \frac{\partial \mathbf{X}}{\partial s} \right| - 1 \right)^2 ds + \frac{1}{2}c_b \int \left(\frac{\partial^2 \mathbf{X}}{\partial s^2} \right)^2 ds, \quad (7)$$

where the first term, containing c_s , represents stretching or compression of the rod and the second term, containing c_b , represents the bending of the rod. Stretching of the filiform hairs is not significant in the problems of interest, so we use $c_s \gg c_b$. In computations we make $c_s = 10^6 c_b$. The parameter c_b must be determined from experimental data. For the 2-D immersed boundary, that represents the cercus, we select both c_s and c_b very large. As a consequence the 2-D boundary is practically immobile.

The inertial force play a key role in response of the hair to the motion of the fluid. We will incorporate the gravitational force \mathbf{F}_K using the massive immersed boundary. The equation for the massive immersed boundary is Newton's law ($\mathbf{F} = m\mathbf{a}$), and the only forces are gravity and a stiff spring force linking the massive and elastic immersed boundary. The location of the massive immersed boundary is given by $\mathbf{Y}(s,t)$, so Newton's law takes the form:

$$M(s) \frac{\partial^2 \mathbf{Y}}{\partial t^2} = -\mathbf{F}_K(s,t) - M(s)\mathbf{g}, \quad (8)$$

where \mathbf{g} is the gravitational acceleration and $M(s)$ is the mass density of the 1-D immersed boundary. The massive and elastic 1-D boundaries are linked by stiff springs with zero rest length and spring constant K . Therefore, the force density for the massive boundary is

$$\mathbf{F}_K = K(\mathbf{Y}(s,t) - \mathbf{X}(s,t)). \quad (9)$$

Larger values of K cause the two boundaries to be linked more closely, but K cannot be set to infinity. Suggested values for K and the accuracy implications of different values are discussed in [20].

In addition to matching the forces between the fluid and the immersed boundary, the velocity of the boundary must also

be approximately equal to the velocity of the fluid. As with the forces described previously, a discrete form of the Dirac delta function is used to handle the interaction between the fluid and solid resulting in the following matching condition:

$$\frac{\partial \mathbf{X}(r,s,t)}{\partial t} = \int \mathbf{u}(\mathbf{x},t) \delta(\mathbf{x} - \mathbf{X}(r,s,t)) d\mathbf{x}. \quad (10)$$

Notice that matching the velocity of the 2-D boundary with that of the fluid, coupled with elastic energy with high c_s and c_b results in no-slip boundary condition on the 2-D boundary.

In summary, equations (2-10) are the full set of equations for the penalty immersed boundary method used here. The only significant, unknown parameter needed to model filiform hair motion is c_b , which must be determined from experimental data.

A number of different numerical approaches have been developed for approximately solving equations systems similar to the one presented in this section [17,21–23]. The formal second-order method used here was originally described in [24] and [18], and a detailed application to the penalty immersed boundary method can be found in [20]. The term *formal* is used because full second-order accuracy is not achieved due to the jumps in the velocity derivative across the immersed boundary. We want to make two additional remarks before briefly describing the algorithm: (1) forward differencing is used for the time derivatives and second-order accuracy is achieved using the midpoint rule so the algorithm presented below is completed twice per time step (i.e., second-order Runge-Kutta), and (2) second-order central finite differences are used for both first and second derivatives in space.

Numerical Algorithm.

Given \mathbf{u} , \mathbf{X} , and \mathbf{Y} from a previous solution or initial conditions, the following algorithm is repeated twice each time step.

1. Update the position of the massless boundary (equation 10).
2. Calculate the force density, which is the sum of the elastic force density (equation 6) and the massive boundary (equation 9).
3. Convert from the force density defined on the Lagrangian grid to forces applied to the Navier-Stokes equations on the Eulerian grid (equation 5).
4. Update the fluid velocity by solving the Navier-Stokes equations (2,3) using a Fast Fourier Transform (FFT). To accomplish this, the velocities from the previous time step are used in the nonlinear convection term ($\mathbf{u} \cdot \nabla \mathbf{u}$).
5. Update the massive boundary (equation 8).

The use of the FFT algorithm requires periodic boundary conditions. This is not a significant limitation because we are able to immerse any boundary we require in the the fluid domain and impose 'inflow velocities' as described in the following section.

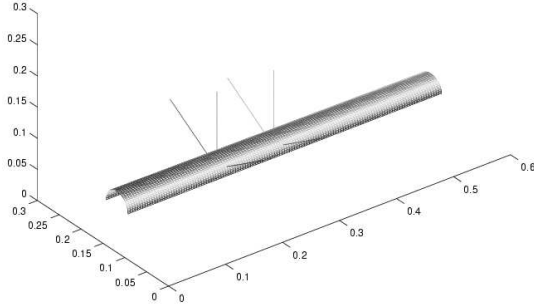


Figure 2. DOMAIN WITH TWO KINDS OF IMMERSIED BOUNDARIES. THE FLUID DOMAIN CONTAINING TWO DIMENSIONAL SURFACE OF A CERCIUS AND FOUR ONE-DIMENSIONAL FILIFORM HAIRS OF VARIOUS LENGTHS. THE DISTANCES ARE GIVEN IN CENTIMETERS.

Model specification for cercal filiform hairs

The model domain is a cuboid with a height of 3 mm , a depth of 3 mm , and a length of 6 mm . The finite difference nodes are equally spaced in all three dimensions, and a typical mesh has $32 \times 32 \times 64$ nodes. A mesh with $64 \times 64 \times 128$ nodes gave nearly identical results. Figure 2 shows the two different types of boundaries immersed in the fluid domain. The two-dimensional cylindrical surface represents the cerci. As explained above, the combination of high c_b and c_s , with the velocity matching imposes no-slip boundary condition on the cercus. This boundary does not extend out to the edges of the domain because then the no-slip condition would conflict with the uniform inflow velocity.

The second type of boundary are one-dimensional filiform hairs that are attached slightly below the cerci surface and are sloped at approximately 80° relative to the cerci surface. The hairs are massive with the mass density set to be that of water [6]. The two bottom nodes on the hair (nearest the center of the cerci) are fixed so that the hair cannot freely rotate without an associated energy cost.

To limit the motion of the hairs to a single plane with a normal vector \mathbf{n} , the velocity of the fluid on the surface of the hair is projected onto the plane of allowed motion by

$$\mathbf{u}_p = \mathbf{u} - (\mathbf{u} \cdot \mathbf{n})\mathbf{n}. \quad (11)$$

The projection has no impact on the velocity field, but the hair only ‘feels’ the projected velocity, \mathbf{u}_p , pushing it in an allowed direction. This is equivalent to projecting out any hair movement

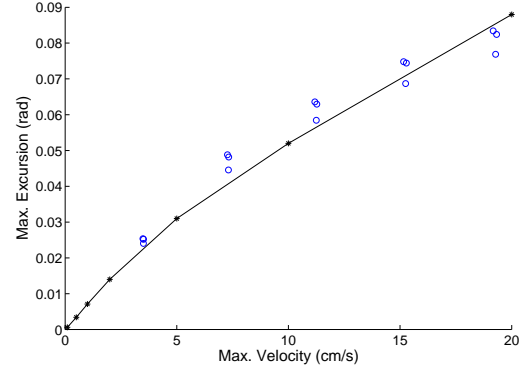


Figure 3. MAXIMAL EXCURSION OF THE HAIR AS A FUNCTION OF THE DRIVING AMPLITUDE FOR $700\mu\text{m}$ HAIR AT 50 HZ DRIVING FREQUENCY. THE LINE INDICATES THE RESULTS OF THE SIMULATION, THE BLUE DOTS REPRESENT THE DATA.

that is not in the allowed plane of motion. Finally, the nodal spacing for the immersed boundaries are set to be less than half the nodal spacing in the fluid to avoid ‘leaks’.

The inflow velocity is set by applying an external force per unit volume on the fluid that is equal to

$$\mathbf{f}_0(\mathbf{x}, t) = \begin{cases} \alpha(\mathbf{u}_0(t) - \mathbf{u}(\mathbf{x}, t)) & , \mathbf{x} \in \Omega_0 \\ 0 & , \text{otherwise} \end{cases}, \quad (12)$$

where $\mathbf{u}_0(t)$ is the desired velocity and Ω_0 is a set points on two grid planes on which we want to control the velocity. For the insects, we are typically interested in temporally oscillating velocities which may approximate velocities created by the flapping wings of a digger wasp as it approaches a cricket. As a result, \mathbf{u}_0 is typically defined by:

$$\mathbf{u}_0(t) = U \cdot \sin(2\pi\omega t) \quad (13)$$

where ω is the frequency of the oscillation and U is the peak velocity (e.g., 1 cm/s).

Results

The first set of numerical experiments were designed to determine the bending stiffness c_b of the cricket hair as a function of position along the length of the hair. This is the one unknown parameter in the model. It has been well established experimentally, that the hair is relatively rigid and bends primarily at the base and beneath the surface of the cerci. We chose the following function to describe the bending stiffness of the cricket filiform

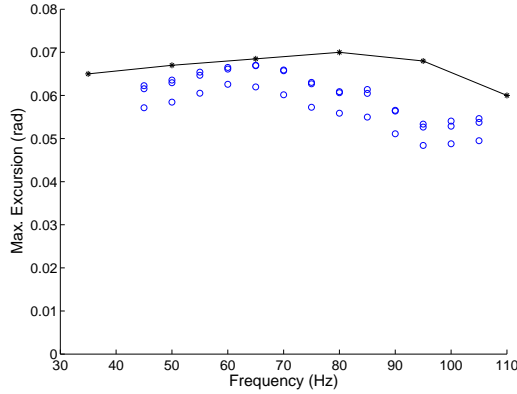


Figure 4. MAXIMUM DEFLECTION AS A FUNCTION OF DRIVING FREQUENCY. THE DRIVING VELOCITY AMPLITUDE IS FIXED AT 10 cm/sec. THE LINE INDICATES THE RESULTS OF THE SIMULATION, THE BLUE DOTS REPRESENT THE DATA.

hair:

$$c_b = \begin{cases} 0.004 & \text{if } x < 0.2 \\ 0.004 + 0.04(1 - \exp(-(10x - 0.2)/L)) & \text{if } x \geq 0.2 \end{cases} \quad (14)$$

The choice of the form comes from [1]. While the choice (14) is based on the present data from measurement in cricket *Acheta domestica*, the model in [1] is based on published data by Kumagai et al. [4] in a different species of cricket *Gryllus bimaculatus*. The only difference between the choice of c_b in these two species is that for *Gryllus* numbers 0.004 in equation 14 are replaced by 0.002 and 0.04 by 0.02. However, the functional form (14) is identical for *Gryllus* and *Acheta*. This implies that the stiffness of the hairs in *Acheta* appears to be twice as large as the stiffness in *Gryllus*. This could be the result of different developmental constraints, or it could be an artifact of different experimental protocols. More experimental work is needed to disambiguate these factors.

With c_b fixed we proceed to test our model against the data.

In the first figure 3 we keep frequency of the stimulus constant at 50 Hz and the hair length is 700 μ m. We change the amplitude U_0 of the sinusoidal background velocity and we measure the maximal excursion of the moving hair. Since the data have been collected in linear regime where the driving velocity amplitudes U_0 are low enough so that the hairs do not come close to their physically imposed limits of motion, we expect that the maximal excursion will change linearly with the driving amplitude. We see that the model (line) matches quantitatively the data (blue circles) well. Also notice that our model also matches linear tendency in the data, that becomes slightly tapered at high driving amplitudes.

In the figure 4 we graph the maximum deflection of a

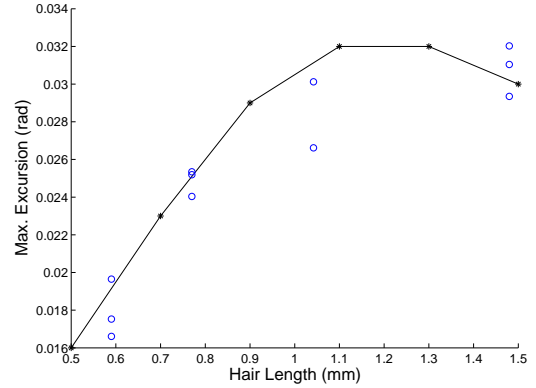


Figure 5. MAXIMAL DEFLECTION AS A FUNCTION OF LENGTH OF THE HAIR. THE INPUT IS FIXED WITH MAXIMAL VELOCITY AMPLITUDE 10 cm/sec AND FREQUENCY 50 Hz. THE LINE INDICATES THE RESULTS OF THE SIMULATION, THE BLUE DOTS REPRESENT THE DATA.

700 μ m hair as a function of the frequency of the driving input, while keeping its maximal velocity amplitude constant as $U_0 = 10$ cm/sec. Both graphs exhibit same qualitative features. Data show maximal deflection around 65 Hz while the simulation has maximum at 80 Hz. This difference and the slightly larger deflections seen overall in the model are probably due to the uniform hair diameter used in the model. The real hairs have tapered parabolic shape [12] and thus they present smaller profile to the moving air.

In figure 5 we fix the input (maximal velocity amplitude is a 4 cm/sec and frequency at 50 Hz) and change the hair length (horizontal axis). On the vertical axis we graph the maximal deflection of the hair. The fit for both the shorter hairs and the long hair is very good.

Finally, in figure 6 we graph the phase shift as a function of frequency, while the maximal velocity amplitude of the input is fixed at 10 cm/sec. Here the phase shift is the difference between the phase of the driving signal and the phase of the response of the hair. We rescale the phase so that it lies on a unit circle and so the horizontal axis should be viewed mod 1.

Conclusions

In this paper we reviewed a penalty immersed boundary method, that was originally proposed in [1]. This method allows simulation of a large number of filiform hairs and is a first step to asking questions about the function of the entire sensory systems consisting of the filiform hairs. In the first paper [1] we fit the model to the data from cricket *Gryllus bimaculatus*, while in this contribution we fit the data to a different species of the cricket *Acheta domestica*. We observed that a change in a single

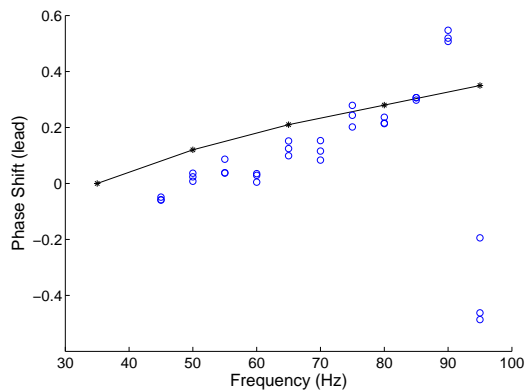


Figure 6. PHASE SHIFT AS A FUNCTION OF FREQUENCY. THE HAIR LENGTH IS $700\mu\text{m}$ AND MAXIMAL VELOCITY AMPLITUDE OF THE INPUT IS FIXED AT 10 cm/s . THE LINE INDICATES THE RESULTS OF THE SIMULATION, THE BLUE DOTS REPRESENT THE DATA.

parameter that models stiffness of the hairs can account for the difference between these species. This shows that our method is very robust, since it is able to fit different data sets with the same structure of the equations.

ACKNOWLEDGMENT

T. G. was partially supported by NSF-CRCNS grant 0515290, NIH-NCRR grant PR16445 and NSF/NIH grant 0443863. J.J.H. was supported by the Flight Attendants Medical Research Institute. B.C.K was supported by the Fulton Undergraduate Research Initiative. J. M-R. was supported by NSF-CRCNS grant 0515290. Any opinions, findings, and conclusions or recommendations expressed in this material are those of the author(s) and do not necessarily reflect the views of the National Science Foundation. We want to thank J.P. Miller for kindly sharing with us the image in Figure 1.

REFERENCES

[1] Heys, J. J., Knott, B., and Gedeon, T., 2007. "Modeling arthropod filiform hair motion using the penalty immersed boundary method". *Bulletin of Mathematical Biology-in review*.

[2] Shimozawa, T., and Kanou, M., 1984. "Varieties of filiform hairs: range fractionation by sensory afferents and cercal interneurons of a cricket". *J. Comp. Physiol. A*, **155**, pp. 485–493.

[3] Shimozawa, T., and Kanou, M., 1984. "The aerodynamics and sensory physiology of range fractionation in cercal filiform sensilla of the cricket *Gryllus bimaculatus*". *J. Comp. Physiol. A*, **155**, pp. 495–505.

[4] Kumagai, T., Shimozawa, T., and Baba, Y., 1998. "Mobilities of the cercal wind-receptor hairs of cricket, *Gryllus bimaculatus*". *J. Comp. Physiol. A*, **183**, pp. 7–21.

[5] Shimozawa, T., Kumagai, T., and Baba, Y., 1998. "Structural scaling and functional design of the cercal wind-receptor hairs of cricket". *J. Comp. Physiol. A*, **183**, pp. 171–186.

[6] Humphrey, J., Devarekonda, R., Iglesias, I., and Barth, F., 1993. "Dynamics of arthropod filiform hairs. i. mathematical modelling of the hair and air motions". *Phil. Trans. R. Soc. Lond. B*, **340**, pp. 423–444.

[7] Barth, F., Wastl, U., Humphrey, J., and Devarakonda, R., 1993. "Dynamics of arthropod filiform hairs. ii. mechanical properties of spider trichobothria (*Cupiennius salei* keys.)". *Phil. Trans. R. Soc. Lond. B*, **340**, pp. 445–461.

[8] Devarakonda, R., Barth, F., and Humphrey, J., 1996. "Dynamics of arthropod filiform hairs. iv. hair motion in air and water". *Phil. Trans. R. Soc. Lond. B*, **351**, pp. 933–946.

[9] Bathellier, B., Barth, F., Albert, J., and Humphrey, J., 2005. "Viscosity-mediated motion coupling between pairs of trichobothria on the leg of the spider *Cupiennius salei*". *J. Comp. Physiol. A*, **191**, pp. 733–746.

[10] Cummins, B., Gedeon, T., Klapper, I., and Cortez, R., 2007. "Interaction between arthropod filiform hairs in a fluid environment". *J. Theoretical Biol*, to appear.

[11] Landolfa, M., and Miller, J., 1995. "Stimulus-response properties of cricket cercal filiform receptors". *J. Comp. Physiol. A*, **177**, pp. 749–757.

[12] Kumagai, T., Shimozawa, T., and Baba, Y., 1998. "The shape of wind-receptor hairs of cricket and cockroach". *J. Comp. Physiol. A*, **183**, pp. 187–192.

[13] Walthall, W., and Murphey, R., 1986. "Positional information, compartments and the cercal system of crickets". *Dev. Biol.*, **113**, pp. 182–200.

[14] Landolfa, M., and Jacobs, G., 1995. "Direction sensitivity of the filiform hair population of the cricket cercal system". *J. Comp. Physiol. A*, **177**, pp. 759–766.

[15] Peskin, C., 2002. "The immersed boundary method". *Acta Numerica*, **11**, pp. 479–517.

[16] Peskin, C., 1977. "Numerical analysis of blood flow in the heart". *J. Comput. Phys.*, **25**, pp. 220–252.

[17] Peskin, C., and McQueen, D., 1995. "A general method for the computer simulation of biological systems interacting with fluids". *Symposia of the Society for Experimental Biology*, **49**, pp. 265–276.

[18] Lai, M.-C., and Peskin, C., 2000. "An immersed boundary method with formal second-order accuracy and reduced numerical viscosity". *J. Comput. Phys.*, **160**, pp. 705–719.

[19] Zhu, L., and Peskin, C., 2002. "Simulation of a flapping flexible filament in a flowing soap film by the immersed boundary method". *J. Comput. Phys.*, **179**, pp. 452–468.

[20] Kim, Y., 2003. "The penalty immersed boundary method

- and its applications to aerodynamics”. PhD thesis, New York University.
- [21] Lee, L., and LeVeque, R., 2003. “An immersed interface method for incompressible Navier–Stokes equations”. *SIAM J. Sci. Comput.*, **25**, pp. 832–856.
- [22] Liu, W., Liu, Y., Farrell, D., Zhang, L., Wang, X., Fukui, Y., Patankar, N., Zhang, Y., Bajaj, C., Lee, J., Hong, J., Chen, X., and Hsu, H., 2006. “Immersed finite element method and its applications to biological systems”. *Comp. Meth. Appl. Mech. Eng.*, **195**, pp. 1722–1749.
- [23] Dillon, R., Fauci, L., Fogelson, A., and Gaver, D., 1996. “Modeling biofilm processes using the immersed boundary method”. *J. Comput. Phys.*, **129**, pp. 57–73.
- [24] Peskin, C., and McQueen, D., 2001. *Heart Simulation by an Immersed Boundary Method with Formal Second-order Accuracy and Reduced Numerical Viscosity*. Kluwer Academic Publishers.